The Journal of Experimental Biology **198**, 2293–2305 (1995)
Printed in Great Britain © The Company of Biologists Limited 1995

MECHANICAL CONTROL OF SWIMMING SPEED: STIFFNESS AND AXIAL WAVE FORM IN UNDULATING FISH MODELS

MATTHEW J. McHENRY[1], CHARLES A. PELL[2] AND JOHN H. LONG JR[1,*]

[1]*Department of Biology, Vassar College, Poughkeepsie, NY 12601, USA* and [2]*BioDesign Studio, Duke University, Durham, NC 27706, USA*

Accepted 14 July 1995

Summary

The purpose of this study was to investigate the mechanical control of speed in steady undulatory swimming. The roles of body flexural stiffness, driving frequency and driving amplitude were examined; these variables were chosen because of their importance in vibration theory and their hypothesized functions in undulatory swimming. Using a mold of a pumpkinseed sunfish *Lepomis gibbosus*, we cast three-dimensional vinyl models of four different flexural stiffnesses. We swam the models in a flow tank and powered them *via* the input of an oscillating sinusoidal bending couple in the horizontal plane at the posterior margin of the neurocranium. To simulate the hydrodynamic conditions of steady swimming, drag and thrust acting on the model were balanced by adjusting flow speed. Under these conditions, the actuated models generated traveling waves of bending. At steady speeds, the motions of the ventral and lateral surfaces of the model were video-taped and analyzed to yield the following response variables: tail-beat amplitude, propulsive wavelength, wave speed and depth of the trailing edge of the caudal fin. Experimental results showed that changes in body flexural stiffness can control propulsive wavelength, wave speed, Froude efficiency and, in consequence, swimming speed. Driving frequency can control tail-beat amplitude, propulsive wavelength, Froude efficiency, relative rate of working and, in consequence, swimming speed. Although there is no significant correlation between rostral amplitude and swimming speed, rostral amplitude can control swimming speed indirectly by controlling tail-beat amplitude and relative power. Compared with live sunfish using undulatory waves at the same speed, models have a lower Froude efficiency. On the basis of the mechanical control of swimming speed in model sunfish, we predict that, in order to swim at fast speeds, live sunfish increase the flexural stiffness of their bodies by a factor of two relative to their passive body stiffness.

Key words: stiffness, undulation, speed, mechanical modeling, swimming, fish.

Introduction

In order to swim, fish transfer momentum to the surrounding water by passing waves of bending down their bodies. By changing the shape and speed of these traveling waves, they modulate the mechanical rate of working and hence control swimming speed (Lighthill, 1975; Videler, 1993). Thus, in order to understand the control of swimming speed, we must investigate the mechanical determinants of the shape and speed of the propulsive undulatory wave.

To swim steadily at faster speeds, teleostean fishes increase both tail-beat frequency and tail-beat amplitude at slow speeds and only tail-beat frequency at higher speeds (e.g. Bainbridge, 1963; Hunter and Zweifel, 1971; Webb, 1988). The length of the propulsive wave is also modulated with changes in steady swimming speed in lake sturgeon *Acipenser fulvescens* (Webb, 1986). Together, these three kinematic variables describe the shape and speed of the undulatory wave and, along with the caudal fin trailing edge depth, are proportional to the mechanical power of the propulsive wave in elongated-body theory (Lighthill, 1975; Wu, 1977). The goals of this study were to determine how these axial wave variables interact mechanically and how they may be altered by changes in the mechanical properties of the body to control swimming speed. Because of the difficulties in the artificial control of muscle activity and passive mechanical properties in fish bodies (Long *et al.* 1994), we built vinyl models of pumpkinseed sunfish *Lepomis gibbosus*, swam them at steady speeds in a flow tank and measured the wave kinematics of their axial midline.

Wave mechanics

Blight (1976, 1977) suggested that the precaudal region of

*Author for correspondence.

a fish's body could function as a wave generator. This idea was deduced from the electromyographic patterns of swimming newt larvae, whose ipsilateral locomotor muscles were simultaneously active during steady undulation. Furthermore, when freshly killed anuran larvae were actuated to swim with an anterior bending couple (Wassersug and Hoff, 1985), their kinematics and pattern of vortex shedding were qualitatively similar to those of live larvae. While steadily swimming fish activate axial muscles sequentially in a rostro-caudal direction (e.g. Jayne and Lauder, 1995; Williams *et al.* 1989; Van Leeuwen *et al.* 1990), the mechanical plausibility of Blight's hypothesis was supported by direct stimulation of the precaudal muscles of dead pumpkinseed sunfish, which generated undulatory waves that produced steady swimming by virtue of their passive propagation down the body (Long *et al.* 1994). The electrically stimulated fish swam at slower speeds than live fish swimming at the same tail-beat frequency, suggesting a role for the caudal muscles in modulating the wave form and producing or transmitting thrust power.

According to Blight's model, the precaudal musculature serves as an oscillator, and the swimming fish is a driven structure. The behavior of driven structures with constant mass and stiffness is governed by simple mechanical principles (Den Hartog, 1934). It seems unlikely, however, that simple mechanics could apply to swimming fish, given the complexities of the external hydrodynamic loading and the internal neuromuscular control. For example, the effective mass of the fish may include the added mass of the water (Denny, 1988). Furthermore, it has been suggested that fish use negative muscle work to vary body stiffness (Altringham *et al.* 1993; Van Leeuwen *et al.* 1990). Indeed, the internal, mechanical drive system is complex, with axial muscle activated by segment rather than by absolute position (Jayne and Lauder, 1995). When calculated from hydrodynamic loads, the pattern and magnitude of internal bending moments are predicted to vary by region (Cheng and Blickhan, 1994*a*). The motive region of the fish's body, they predict, produces a standing wave of bending moment and is located just posterior to the largest cross-sectional area of muscle. The caudal muscles, in contrast, are thought to generate a smaller but traveling wave of bending moment (Cheng and Blickhan, 1994*a*). Given these complexities, and our lack of knowledge about their interactions, simple mechanical principles can provide a basis for functional predictions, which, in turn, can be tested experimentally.

In simple mechanical terms, the speed (c) of a wave traveling through a solid or fluid is the product of the frequency of the wave (f) and its wavelength (λ):

$$c = f\lambda\,, \tag{1}$$

where the speed of the wave is constant as long as mass and stiffness are conserved (Halliday *et al.* 1993). Under these conditions, increases in wave frequency must result in a decrease in the wavelength. Not surprisingly, swimming teleosts violate these simple assumptions: as wave frequency (measured by tail-beat frequency) increases with increasing swimming speed, the propulsive wavelength is held constant (e.g. Bainbridge, 1963; Webb, 1988). On the basis of this discrepancy, one can make the following prediction: in order to change the speed of its propulsive wave, an undulatory swimmer must change the flexural stiffness of its body.

In a similar fashion, we can predict the relationship between the tail-beat amplitude and the wave frequency. In a driven oscillatory system, the amplitude of the wave is greatest at the system's resonance frequency, which is a function of its mass and stiffness (Den Hartog, 1934; Halliday *et al.* 1993). Wave amplitude increases as the driving frequency approaches the resonance frequency of the system. Swimming teleostean fish appear to violate the assumptions of this principle. While tail-beat amplitude increases as the fish changes from slow to medium-fast swimming speeds, the amplitude is kept constant as the fish swims at even faster speeds with increasing tail-beat frequency (Bainbridge, 1963; Webb, 1986). Wave amplitude is also dependent on the driving amplitude of the oscillator (Den Hartog, 1934). In live pumpkinseed sunfish, the lateral amplitude of the rostrum, which may be an indicator of driving amplitude, increases with increasing swimming speed (Long *et al.* 1994). We can, therefore, make a second functional prediction: in order to maintain a constant tail-beat amplitude with increasing frequency, an undulatory swimmer must increase the stiffness of its body and/or the driving amplitude of its anterior oscillator.

In addition to predictions of wave-form control, how the wave form affects swimming speed can be predicted from hydromechanical theory. Using Lighthill's elongated-body theory (for a review, see Lighthill, 1975; Videler, 1993), Wu (1977) showed that the mechanical rate of working of the undulatory wave, P, is proportional to the following variables:

$$P \propto F^2H^2B^2\left(1 - \frac{u}{c}\right), \tag{2}$$

where F is the tail-beat frequency, H is the tail-beat amplitude, B is the depth of the trailing edge of the caudal fin, u is the forward swimming speed and c is the rearward speed of the undulatory wave, which is the product of tail-beat frequency and propulsive wavelength, λ. From this relationship, we predict that, in order to swim faster, an undulatory swimmer will increase its total rate of working by modulating its axial wave motion as predicted by elongated-body theory. Note that, under this scenario, body stiffness and driving amplitude would act to control swimming speed indirectly by controlling wave motion directly, as predicted above.

In order to test these predictions we needed an experimental system in which the investigator could control the driving frequency, driving amplitude and stiffness of the body while holding mass and hydrodynamic conditions constant. Since this approach is difficult with live or dead fish, we built mechanical fish models of varying stiffness that mimic many of the characteristics of live fish: they swim by generating undulatory waves, they approximate the flexural stiffness of the body and they match its external morphology. They also

match the pattern, but not the magnitude, of the axial input of bending moments predicted for a carangiform swimmer (Cheng and Blickhan, 1994*a*).

Materials and methods

Construction of models

A 12.2 cm long (from rostrum to tail fork) pumpkinseed sunfish was killed with an overdose of tricaine (MS-222, Argent Chemical Laboratories). After removal of the superficial mucus layer (using household detergent), the fins were fixed by applying a formalin solution. Median fins were fully extended in the mid-sagittal plane and paired fins were fully adducted. Prior to molding the fish, the body was set in a neutral position, with no detectable lateral curvature (median line of fish less than 1 mm away from a straight line) with the mouth fixed shut. This procedure was completed in 10 min.

The prepared fish was molded using a quick-setting silicone elastomer (Silicones Incorporated GI-1000 resin and Ultrafast catalyst). The cured mold was used to cast fish replicas made of polyvinyl chloride gel (PVC, MF Manufacturing Co., stock 3228H-5 B.F.). The molten virgin PVC (193 °C) was poured into the mold cavity, solidifying around a rigid block of material suspended in the cranial region. A drive shaft connected to this stiff region, at an axial position of 25 % of the total length and perpendicular to the long axis of the model, transmitted an oscillatory bending moment which served to actuate the models (Fig. 1). This position for the input of a standing, oscillatory bending moment roughly corresponds (see Fig. 2) to the position of the 'motive' region just posterior to the largest cross-sectional muscle area in carangiform fish (Cheng and Blickhan, 1994*a*). Four models were cast, each identical in external morphology but different in body stiffness. Body stiffness was varied by addition of diluent (MF Manufacturing Co., stock 4116S) to the PVC. The PVC gel compound varied from 40 % diluent (by mass) in the least stiff fish to 10 % diluent in the stiffest fish.

Body flexural stiffness

Body stiffness was measured with a dynamic bending machine modified after Long (1992). A small region (11 % of body length) between the neurocranium and pectoral girdle was bent in each of four models with a sinusoidal angular displacement at three cycle frequencies that matched experimental swimming frequencies of 2, 3 and 4 Hz (see below). Angular displacement, set at ±10 ° for these dynamic tests, was monitored using a rotary variable differential transducer (Schaevitz, model R30D). The bending moment (N m) needed to cause the angular motion was measured using a half-bridge strain gauge and bridge amplifier (Omega Engineering, model DMD-520). Both signals were sampled digitally at 20 Hz (Vernier Inc., Universal Laboratory Interface). Since the models were built of an isotropic, homogeneous material (PVC), the bending stiffness of the body was characterized by the flexural stiffness, EI (N m^2), where E is the Young's modulus of elasticity (N m^{-2}) and I is the second moment of area (m^4), a shape factor that accounts for the placement of the cross-sectional area relative to the bending axis (Wainwright *et al.* 1976). First, we calculated E at each bending frequency for each model according to the following formula (Denny, 1988):

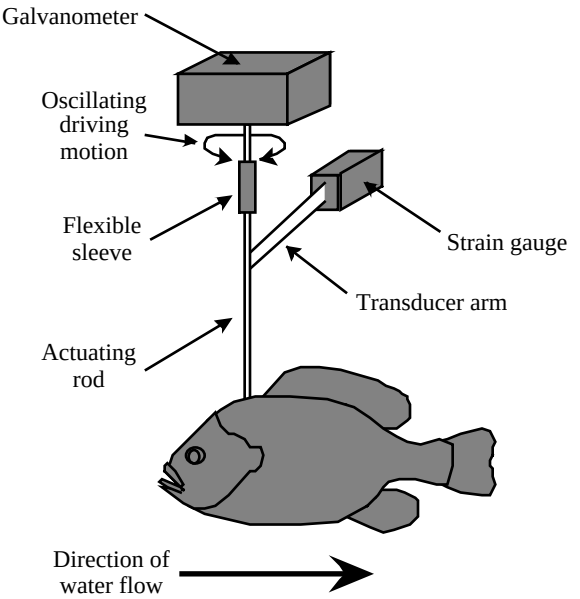

Fig. 1. Swimming model in a flow tank. Model sunfish generated thrust when an oscillating, sinusoidal bending couple was transferred from the galvanometer *via* an actuating rod with a single linkage to the model. The amplitude and frequency of the bending couple were altered by varying the signal from a function generator. The anterior bending couple produced a standing bending moment wave anteriorly that produced a traveling bending moment wave that propagated caudally and produced thrust (see also Fig. 3). To mimic conditions of steady swimming, thrust was balanced by drag; drag was created by water movement in the flow tank. These two forces were monitored *via* a strain gauge attached to the actuating rod.

$$E = (MR)/I, \tag{3}$$

where M is the bending moment (N m) and R is the corresponding radius of curvature (m) of the portion of the fish being bent. We measured M continuously during bending tests and chose the maximal value of each model to calculate E. The radius of curvature, R, was calculated, using trigonometry, from the maximal bending angle of the section of model test piece, θ, and the section length, L, assuming that the end-points and mid-point of the bending section fell on a circle of constant radius:

$$R = \frac{L}{4\cos(\theta/2)} . \tag{4}$$

The second moment of area, I, was calculated by approximating the body's cross section as an ellipse, measuring the major and minor axes of the ellipse, and then using a standard engineering calculation (Denny, 1988). In this fashion, I was also measured along the length of the model so

that the flexural stiffness, *EI*, could be calculated as a function of axial position. Using the same procedure, *E* was calculated for the caudal region of a dead pumpkinseed sunfish (length 13.0 cm). To test for amplitude effects, models and dead fish were bent quasi-statically over an angular range that exceeded displacements seen during swimming (±30 °).

Swimming of models

We swam the models over a range of speeds in a flow tank (like that described by Vogel, 1981). Flow speed was calibrated and velocity gradients were controlled as described elsewhere (Long *et al.* 1994). In addition to controlling flexural stiffness in the models, the driving frequency and driving input amplitude (as measured by the lateral amplitude of the rostrum) were varied in two different sets of experiments. First, to examine the effects of driving frequency and Young's modulus, all four models were driven at frequencies of 2, 3 and 4 Hz with the rostral amplitude held at 0.50 cm. These driving frequencies and rostral amplitude were chosen because they match those measured in live, steadily swimming pumpkinseed sunfish (Long *et al.* 1994). Second, to examine the effects of driving amplitude, all four models were driven at a frequency of 2 Hz with three different rostral amplitudes: 0.23, 0.35 and 0.50 cm.

The wave input signal was a sinusoidal wave (provided by a function generator, Krohn-Hite, model 1000) amplified (by a NAD model 3200 power amplifier) to drive a galvanometer attached to the actuating rod of the model (Fig. 1). This sinusoidal, oscillating signal produced a torque that generated a standing bending moment in the anterior region of the model. This bending moment caused anterior bending that was transmitted posteriorly in a manner determined by the passive elastic properties of the body and the external hydrodynamic loads. Thus, anteriorly the bending moments are present in a standing wave, while posteriorly they travel towards the tail. This pattern is similar to that predicted for carangiform swimmers from hydrodynamic theory (Cheng and Blickhan, 1994*a*). Without posterior 'muscles', however, the model cannot generate the increased magnitude of bending moment predicted caudally (see Fig. 7, Cheng and Blickhan, 1994*a*).

To mimic hydrodynamic conditions of steady (constant-velocity) swimming, the flow speed for each experiment was adjusted so that thrust and drag were equal and opposite. Thrust and drag were monitored by a strain gauge fitted to the actuating rod and digitally sampled as described above.

The bending couple of the galvanometer was linked to the actuating rod through a 1.0 cm length of flexible rubber tubing. We were concerned that this linkage might limit lateral head movement and create an unrealistic swimming motion. To examine the effect of the flexible linkage, we repeated our experiments using a universal joint linkage, which gave no resistance to lateral movement. The swimming motions generated by each linkage were statistically indistinguishable. The data from the universal joint linkage, however, were less repeatable than those from the flexible linkage. This behavior was caused by the instability of the universal joint and the resulting difficulty in controlling the orientation of the model. As a result, we present only the data from the flexible linkage experiments.

The ventral and lateral surfaces of models and live fish were video-taped at 60 images s^{-1} with an exposure time of 1 ms (Panasonic model AG-450 SVHS camcorder). Ventral midlines from each video field were digitized and analyzed using a computer (Apple Corporation, model Quadra 900), software (National Institutes of Health program Image), superVHS video deck (Panasonic, model AG-1960) and a time-base corrector (Nova, model 800). Digitized video frames were superimposed on a Cartesian coordinate grid, upon which 15 points were traced down the central body axis of the ventral surface. From the lateral view, the caudal fin trailing-edge depth (tail-depth) was measured as described in the next section.

Kinematics

From the digitized midlines of the models, kinematic response variables were measured and used to calculate wave speed, Froude efficiency and the relative mechanical power (Webb *et al.* 1984). By tracking the movement of the tip of the caudal fin, tail-beat amplitude and driving frequency were determined. Tail-beat amplitude (cm) was measured as half the average distance between maximum right and left excursions over three or more tail-beats. Driving frequency (Hz) was the inverse of the average period (s) of three complete tail-beat cycles. To determine propulsive wavelength (λ, cm), we measured the posterior half-wavelength, which yields more accurate measurements than the whole wavelength measured from head to tail (Webb *et al.* 1984). By tracking the anterior-most point of the rostrum, we measured rostral amplitude (cm) as half the average distance between right and left excursions over three or more tail-beats. The caudal fin trailing-edge depth (tail depth, cm) was measured as the vertical distance, in the sagittal plane, between the dorsal- and ventral-most points on the caudal fin. Since the models vary only in material composition, it is possible for tail depth to vary with material stiffness or, as hydrodynamic loads change, with swimming speed.

The speed of the propulsive wave, *c*, was calculated for a given trial as the product of tail-beat frequency and twice the posterior propulsive half-wavelength (equation 1). Froude or propellor efficiency (η), the ratio of thrust power to total rate of working, was calculated using the following equation (Cheng and Blickhan, 1994*b*; Webb *et al.* 1984):

$$\eta = (c + u)/2c\,, \tag{5}$$

where *c* is wave speed and *u* is swimming speed. We also calculated the relative rate of working (or relative power) *P*, of the undulatory wave using equation 2.

Statistical design

To test the hypothesis that the response variables (tail-beat amplitude, propulsive wavelength, tail depth, wave speed and swimming speed) vary with changes in the control variables

(driving frequency, rostral amplitude and Young's modulus), we performed a modified profile analysis of variance (ANOVA), a conservative analysis that minimizes the chance of false significance caused by inflated degrees of freedom (Simms and Burdick, 1988). This analysis is a compromise: a simple regression analysis could not be used because the small number of data points (three or four per trial) limits the ability to detect non-zero slopes on an individual basis; however, merely increasing the number of data points for each individual inflates the degrees of freedom.

To test the effects of driving frequency, each response variable for each of the four models was linearly regressed onto driving frequency. The mean of the four slopes (N=4) was then compared, using a *t*-test, with slopes having a mean and standard deviation of zero. A significance level of $P \leqslant 0.05$ indicated a mean slope significantly different from a slope of zero. The same procedure was repeated for rostral amplitude and each of the response variables in turn. To test the effects of Young's modulus, the same procedure was followed except that the sample size for each test was three, with each frequency (2, 3 and 4 Hz) used as the 'individual'. This *t*-test was two-tailed in cases where we had no *a priori* assumption as to the direction of the effect. Where mechanical theory allowed us to predict a specific outcome, as discussed in the Introduction, a one-tailed *t*-test was used. The following relationships were analyzed using a one-tailed *t*-test: propulsive wavelength as a function of driving frequency and Young's modulus; tail-beat amplitude as a function of rostral amplitude; swimming speed and relative power as a function of driving frequency and rostral amplitude; and wave speed as a function of Young's modulus.

Finally, we compared the models with live pumpkinseed sunfish swimming at similar wave speeds. With wave speed held constant, we compared the swimming speeds and Froude efficiencies of the two propulsive systems. We selected eight trials from the 36 model trials where the mean value of the wave speed was statistically indistinguishable, as determined using a *t*-test, from the mean wave speed of live sunfish swimming at eight different swimming speeds (Long *et al.* 1994). Because wave speed is directly related to hydrodynamic power (equation 2), this test compares the swimming performance of the two different propulsive systems. It is important to note that the behavior of the models and live fish match, as closely as is possible with this experimental system and our current knowledge of live fish mechanics, in both kinematics and bending moment activation pattern. The differences between models and live fish, as far as they can be determined from our limited knowledge of muscle function (see Jayne and Lauder, 1995), are considered further below.

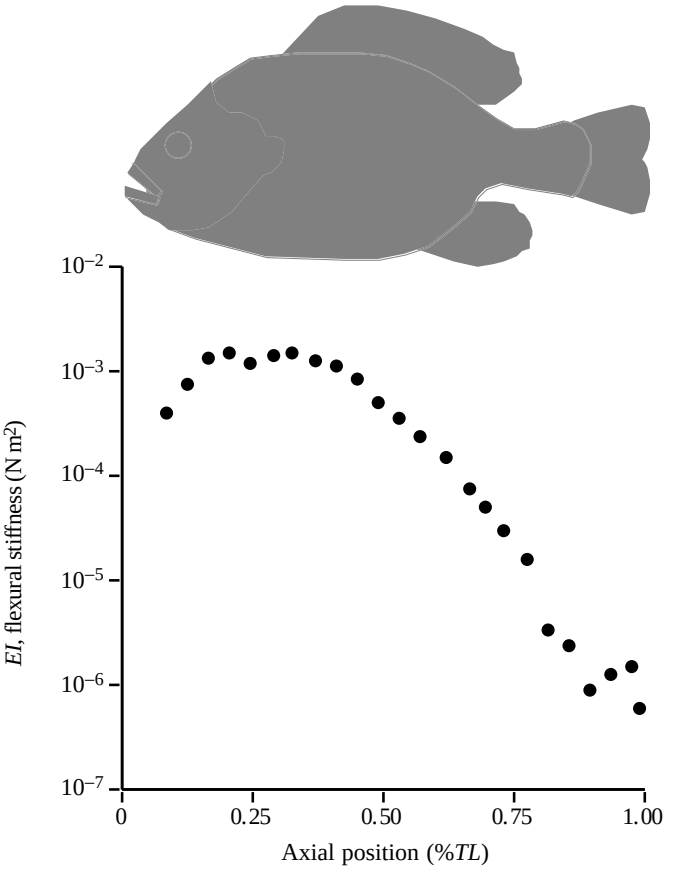

Fig. 2. Flexural stiffness of a model as a function of axial position. Flexural stiffness, *EI*, was calculated using standard engineering formulae (see Materials and methods) and decreases by three orders of magnitude from head to tail. The plotted values are for the second stiffest fish (with a Young's modulus of 0.20 MPa). Note that the shape of the curve is determined by changes in cross-sectional area, which in turn changes the second moment of area, *I* (see equation 3). The shape of the curve is therefore identical in the other models, while the curve's vertical position is shifted vertically in proportion to the model's Young's modulus, *E*. *TL*, total length.

Results

Stiffness of models

The Young's moduli of the four models, measured at a bending frequency of 2 Hz, were 0.16, 0.18, 0.20 and 0.22 MPa. For each model, the Young's modulus increased with increasing bending frequencies of 3 and 4 Hz (at 2, 3 and 4 Hz, Young's modulus for model 1 was 0.16, 0.18, 0.18; model 2 was 0.18, 0.18, 0.20; model 3 was 0.20, 0.20, 0.25; and model 4 was 0.22, 0.22, 0.27, respectively). The flexural stiffness, *EI*, of the models varied from a maximum of 10^{-2} N m^2 near the head to a mimimum of 10^{-6} N m^2 in the tail (Fig. 2). The caudal region of the dead pumpkinseed sunfish was found to have a Young's modulus similar to that of the models: 0.18 MPa at a bending frequency of 2 Hz. No significant effect of frequency was found for the dead sunfish. For both the models and dead fish, no changes in Young's modulus were detected when varying bending amplitude.

Model swimming

Models produce undulatory waves that propagate caudally and generate thrust (Fig. 3). The statistical relationships between the control variables and the kinematic response

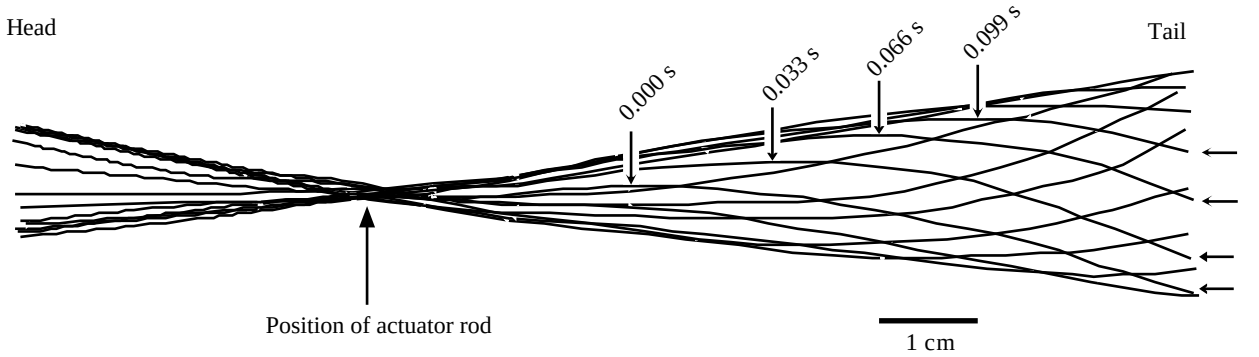

Fig. 3. Undulatory wave motion of a swimming model. Motion of the midline from one tail-beat cycle, as show by superimposed ventral midlines. In this example, the driving frequency was 2 Hz, the rostral amplitude was 0.5 cm and the Young's modulus was 0.22 MPa. The interval between midline images is 0.033 s. The small arrows and labeled times indicate the caudal progression of a wave of bending in the posterior region.

variables are summarized in Table 1. The posterior propulsive half-wavelength decreases with increasing driving frequency (Fig. 4A) in a manner consistent with passive wave theory (equation 1). While constant with respect to changes in rostral amplitude (Fig. 4B), it increases with increasing Young's modulus (Fig. 4C).

Tail-beat amplitude decreases with increasing driving frequency (Fig. 5A). At the same time, tail-beat amplitude increases with increasing rostral amplitude (Fig. 5B) and is statistically independent of Young's modulus (Fig. 5C).

Although tail depth is independent of driving frequency and amplitude, it increases significantly with increasing Young's modulus (Table 1).

Swimming speed decreases with increasing driving frequency (Fig. 6A), is independent of rostral amplitude (Fig. 6B) and increases with increasing Young's modulus (Fig. 6C). The increase in speed with increasing Young's modulus supports the hypothesis that flexural stiffness is an important property in controlling swimming performance.

Propulsive wave speed (equation 1) increases with increasing Young's modulus (Fig. 7). Wave speed was independent of driving frequency and rostral amplitude. Froude efficiency increases with increasing Young's modulus (Fig. 8B) and decreases with increasing driving frequency (Fig. 8A). Froude efficiency is independent of rostral amplitude.

The relative rate of working (or relative power) increases significantly with driving frequency and rostral amplitude (Fig. 9A,B), but is independent of changes in Young's modulus.

How models compare with live fish

When comparing data from models with a mean propulsive wave speed equal to that of live sunfish (N=8, Fig. 10A), swimming speed is significantly lower in the models

Table 1. *How the control variables determine the kinematic response variables*

Response variables	Control variables: Driving frequency (Hz)				Rostral amplitude (cm)				Young's modulus (MPa)			
	Mean	Slope	Intercept	r^2	Mean	Slope	Intercept	r^2	Mean	Slope	Intercept	r^2
Tail-beat amplitude (cm)	–	–0.28±0.069	1.93±0.184	0.98±0.017	–	1.74±0.543	0.42±0.165	0.98±0.011	2.09±0.442	–	–	–
Propulsive half-wavelength (cm)	–	–1.48±1.104	12.63±2.127	0.74±0.276	9.13±0.689	–	–	–	–	26.60±16.604	2.62±5.014	0.57±0.412
Tail depth (cm)	2.48±0.077	–	–	–	2.47±0.100	–	–	–	–	2.88±0.909	1.9±0.138	0.96±0.039
Swimming speed ($cm\,s^{-1}$)	–	–2.17±1.147	20.23±4.155	0.85±0.102	11.9±4.518	–	–	–	–	151.38±4.899	–16.35±6.221	0.69±0.282
Froude efficiency	–	–0.0508±0.015	0.79±0.076	0.91±0.067	0.62±0.056	–	–	–	–	1.34±0.408	0.37±0.037	0.62±0.187
Relative power	–	10.1±6.86	8.9±15.20	0.9±0.162	–	45.4±26.16	6.6±12.28	0.8±0.17	39.2±10.36	–	–	–

The slope, intercept and r^2 values are given for statistically significant relationships and the mean value for non-significant regressions.
Raw data are plotted in Figs 4–9.
Significance was determined using a profile analysis of variance (see Materials and methods).
Values are means ± 1 S.D.; values of N are given in figure legends.

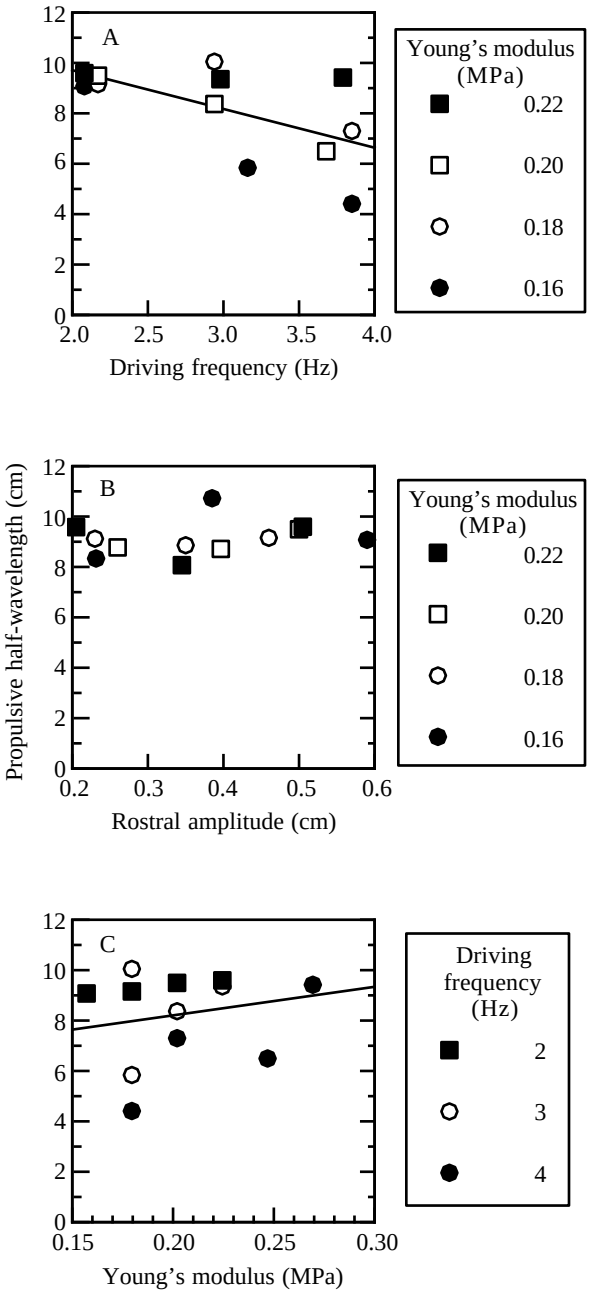

Fig. 4. Propulsive half-wavelength of swimming models. This kinematic variable describes the shape of the undulatory wave and, according to mechanical theory (see Introduction), should change with driving frequency and Young's modulus (which represents body stiffness). Lines represent the mean slope of the three or four data sets, rather than a regression of the pooled data (see Materials and methods for explanation of statistical design). See Table 1 for mean values and regression equations. (A**)** Unlike observed values for live fish, propulsive half-wavelength decreases significantly with increasing driving frequency (N=4, P=0.04). (B) Propulsive half-wavelength is statistically independent of rostral amplitude (N=4, P=0.16), as is the case for live fish. (C) Propulsive half-wavelength increases significantly with increasing Young's modulus (N=3, P=0.05). These data support the hypothesis that body stiffness controls the shape of the undulatory wave.

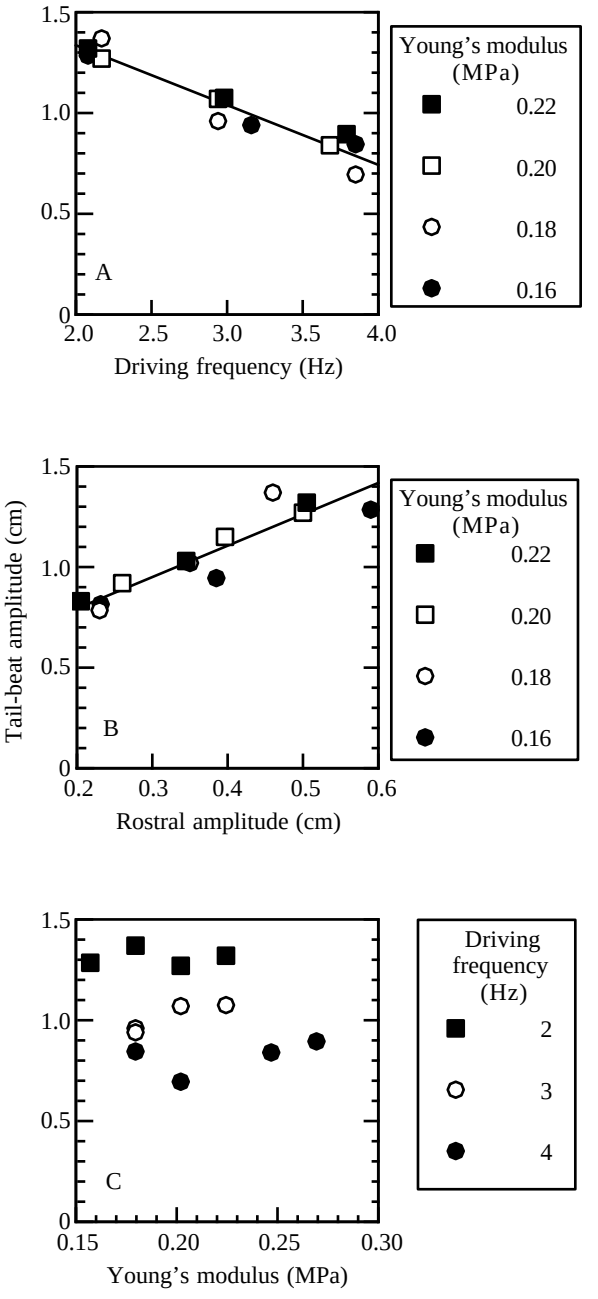

Fig. 5. Tail-beat amplitude of swimming models. This kinematic variable is directly proportional to mechanical power output (see equation 2) and should, according to mechanical theory (see Introduction), change with driving frequency, rostral amplitude and Young's modulus. Lines represent the mean slope of the three or four data sets, rather than a regression of the pooled data (see Materials and methods for explanation of statistical design). See Table 1 for mean values and regression equations. (A) Tail-beat amplitude decreases significantly with increasing driving frequency (N=4, P<0.01). (B) Tail-beat amplitude increases significantly with increasing rostral amplitude (N=4, P=0.01). These data suggest that a live fish could maintain a constant tail-beat amplitude, with increasing tail-beat frequency, by increasing rostral amplitude. (C) Tail-beat amplitude is statistically independent of Young's modulus (N=3, P=0.26).

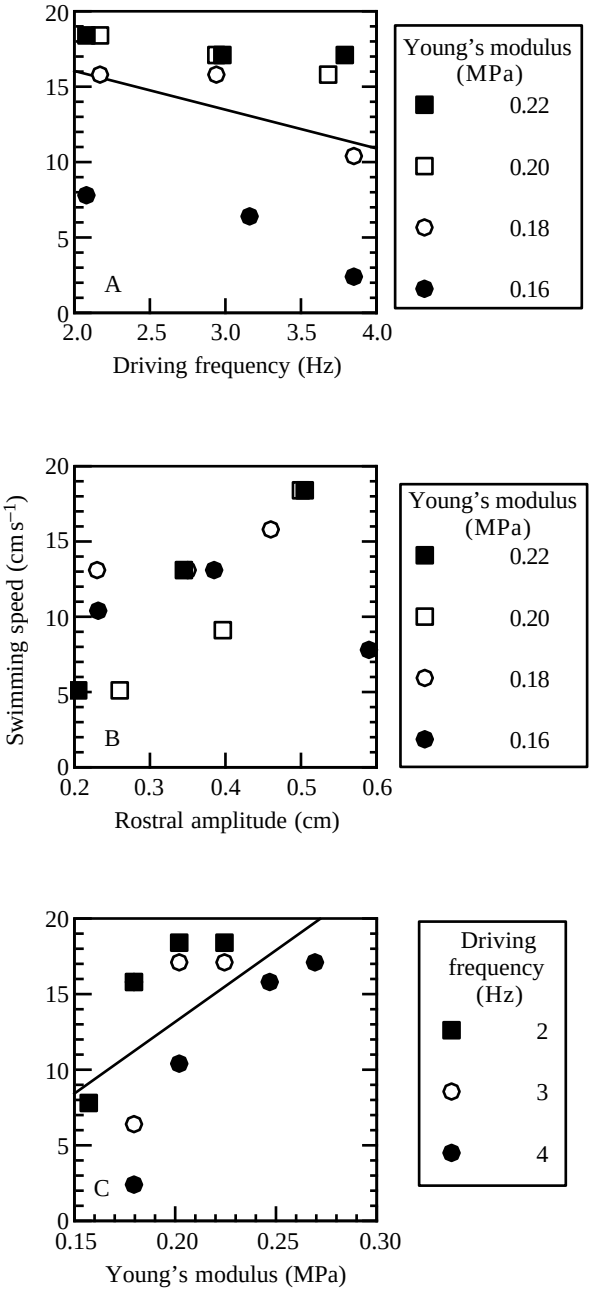

Fig. 6. Swimming speed of swimming models. This performance variable is determined by the interaction of kinematic variables (see Figs 4, 5), efficiency (see Fig. 7) and power (see Fig. 9). Lines represent the mean slope of the three or four data sets, rather than a regression of the pooled data (see Materials and methods for explanation of statistical design). See Table 1 for mean values and regression equations. (A) Swimming speed decreases significantly with increasing driving frequency (N=4, P=0.02). This relationship is consistent with the hypothesis that driving frequencies above 2 Hz are greater than the natural resonance frequency for the system. In live fish, tail-beat frequency and swimming speed are positively correlated. (B) Swimming speed is statistically independent of rostral amplitude (N=4, P=0.09). Live fish increase rostral amplitude with swimming speed. (C) Swimming speed increases significantly with increasing Young's modulus (N=3, P<0.01). These data suggest that live fish increase their body stiffness in order to swim faster.

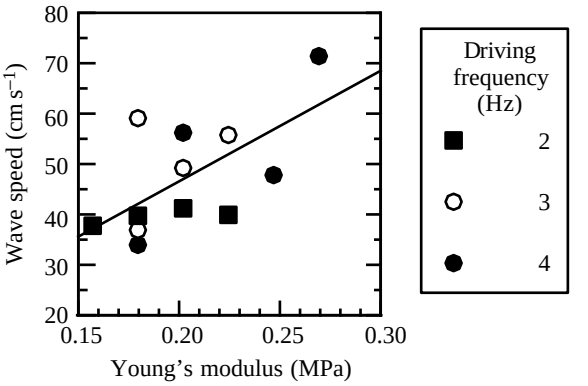

Fig. 7. Wave speed of swimming models. This kinematic variable is the product of driving frequency and the propulsive wavelength. According to mechanical theory, wave speed should be proportional to the body's flexural stiffness (see equation 7). Propulsive wave speed c increases with increasing Young's modulus E (c=2.672+219.458E, r^2=0.415, P=0.05). Wave speed was independent of driving frequency and rostral amplitude; the mean wave speed was 94.83±22.57 cm s^{-1} (±1 S.D.) during the frequency tests and 78.21±6.25 cm s^{-1} (±1 S.D.) during the amplitude tests. It is interesting to note that live fish increase wave speed as they swim faster. That wave speed varied only with Young's modulus in the models suggests that, in order for a live fish to increase its wave speed, it must stiffen its body.

(Fig. 10B). Thus, the Froude efficiency is also significantly lower (Fig. 10C).

Discussion

In steadily swimming sunfish models, swimming speed is controlled by three factors: driving frequency (Hz), rostral amplitude (cm) and the body's Young's modulus (MPa), all of which operate by altering the form of the undulatory wave (Fig. 11). These effects are predicted by simple mechanical theory and provide an empirical basis for predictions of how live fish, which swim more efficiently than models (Fig. 10), mechanically control swimming speed. While the models mimic the pattern of bending moments predicted in carangiform swimmers, without posterior contractile units they do not power the traveling wave of bending in a manner identical to that predicted in fish (Cheng and Blickhan, 1994*a*). Hence, comparisons between the performance of model and live sunfish should be interpreted cautiously.

Control of wave form in models

As predicted by mechanical theory (equation 1), the tendency of increasing driving frequency to reduce propulsive wavelength can be counteracted by increasing Young's modulus, which increases propulsive wavelength (Fig. 4) and wave speed (Fig. 7). Furthermore, increasing driving frequency decreases tail-beat amplitude (Fig. 5A), a result consistent with the hypothesis that the models are operating above their resonance frequency (see Introduction). Tail-beat amplitude, however, was not affected by increases in Young's

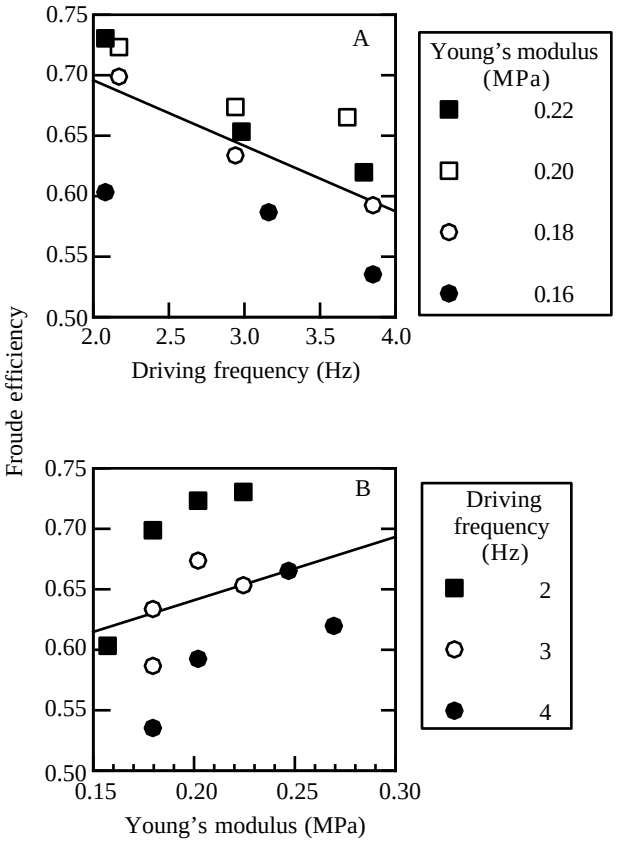

Fig. 8. Froude efficiency of swimming models. This variable is the ratio of useful to total hydrodynamic power generated by the model's undulatory wave (see equation 5). See Table 1 for mean values and regression equations. (A) Froude efficiency decreases linearly with increasing driving frequency (N=4, P=0.01). (B) Froude efficiency increases with increasing Young's modulus (N=3, P=0.03). Froude efficiency was independent of rostral amplitude and had a mean value of 0.576±0.028 (±1 S.D., P=0.19). Once again, these data demonstrate the importance of body stiffness. A model may swim faster by increasing Young's modulus, which increases the proportion of total power used to generate thrust.

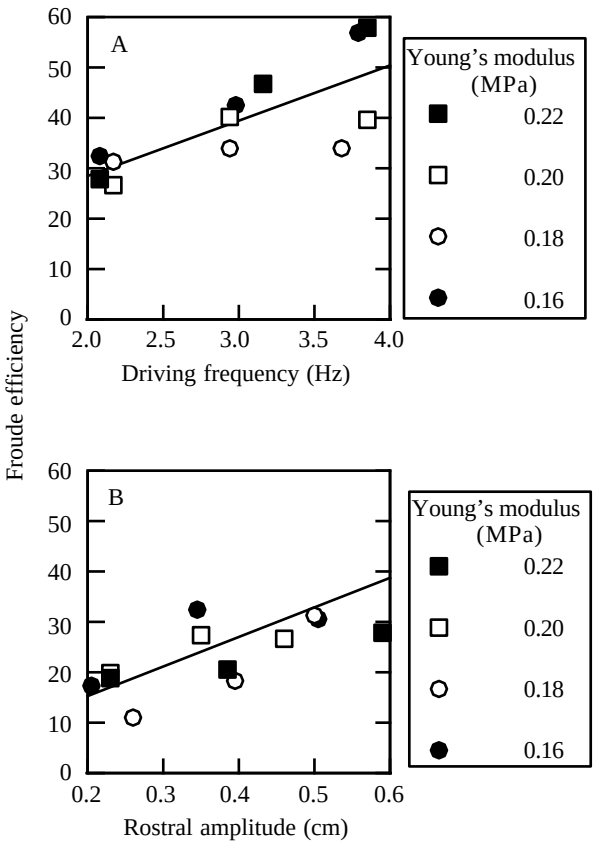

Fig. 9. Relative power of the undulatory wave of swimming models. Relative power is calculated from the kinematic variables of the undulatory wave (see equation 2). See Table 1 for mean values and regression equations. (A) Relative power increases linearly with driving frequency (N=3, P=0.03). (B) Relative power increases linearly with rostral amplitude (N=3, P=0.02). Relative power was independent of Young's modulus.

modulus (Fig. 5C); only increases in rostral amplitude increased tail-beat amplitude.

Control of swimming speed in models

Since steady swimming is achieved when thrust balances drag, speed is determined by the model's ability to produce sufficient thrust power. From the conservation of energy, total mechanical power, P_{tot}, is the power required to overcome the drag, D, at a given swimming velocity, u (Wu, 1977):

$$P_{tot}\eta = Du\,, \tag{6}$$

where η is the Froude efficiency (equation 5), with a value between 1 and 0, and is an index of the useful work done by the propulsive wave (Lighthill, 1975). An efficiency of 1 means that the total power is equal to the thrust power; efficiencies less than 1 mean that some of the total power is lost in the kinetic energy of the wake (Videler, 1993).

In the model fish, Froude efficiency explains the effect of driving frequency on swimming speed (Fig. 6A). From elongated-body theory (equation 2), we would expect an increase in driving frequency to increase the relative rate of working (relative power) of the propulsive wave (Fig. 9A). At the same time, decreasing Froude efficiency (Fig. 8A) decreases thrust power, which causes a reduction in swimming speed in spite of greater total mechanical work. As we saw with swimming kinematics, this effect of increasing driving frequency can be offset by increases in Young's modulus. Young's modulus alone does not affect the relative power output (Table 1); instead, it increases swimming speed by increasing Froude efficiency (Fig. 8B). Thus, in order to swim faster, more total power is generated by increasing driving frequency and a greater proportion of this power is applied to thrust generation by stiffening the body.

How models compare with live fish

Before making predictions of the mechanical control of swimming speed in live fish, it is important to understand the limits of extrapolating from the results of our model fish. Our

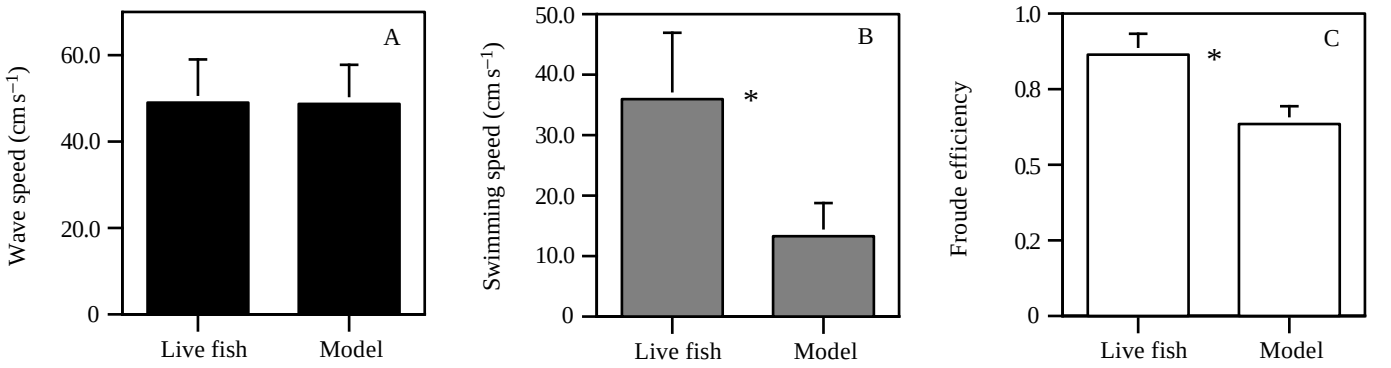

Fig. 10. Fish and model swimming compared. For both live and model categories, N=8. (A) Wave speed. The samples were chosen so that wave speeds would be statistically indistinguishable (paired t-test, P=0.946). There is also no significant difference between mean propulsive wavelength, tail-beat frequency and tail-beat amplitude (paired t-test, P>0.10). (B) The mean swimming speed of models was significantly lower than that of live fish (P=0.001). (C) Model Froude efficiency was significantly lower than that of live fish (P<0.001). This comparison demonstrates that models, when swimming with kinematic parameters equivalent to those of live sunfish, are less efficient swimmers. The efficiency of live sunfish may largely be due to their ability of to generate power along the full length of the body; the models generate power only anteriorly. Significant differences between live fish and the model are marked with an asterisk. Values are means + 1 S.D.

models differ in at least two major ways from live fish. First, they are built of a homogeneous, isotropic material (PVC), whereas the bodies of fish are constructed of a variety of materials in complex, three-dimensional arrangements (Jayne and Lauder, 1994; Videler, 1993; Westneat *et al.* 1993; Wainwright, 1983). Second, the models are actuated by a simple mechanical bending couple just posterior to the neurocranium, whereas the bodies of fish receive mechanical input from muscles extending from the neurocranium to the caudal fin. At the same time, it is also important to realize that the mechanical role of the caudal muscle segments in live fish remains in question (compare Rome *et al.* 1993 with Altringham *et al.* 1993); furthermore, muscle activity propagates by myomere, and not simply by axial position, a fact which, when combined with the complex geometry of muscles, underscores our ignorance of the functional units of undulatory propulsion (Jayne and Lauder, 1995).

Given their simplicity, it is at first surprising that the models swim by generating traveling waves of bending (Fig. 3). This result supports Blight's hypothesis (1976, 1977), that anterior muscles are sufficient to drive undulatory motion, and is consistent with experiments on passively propagated waves in tadpoles (Wassersug and Hoff, 1985) and muscularly driven, passively propagated waves in sunfish (Long *et al.* 1994).

Since the undulatory wave propagates from head to tail, the mechanical properties of the body, and stiffness in particular,

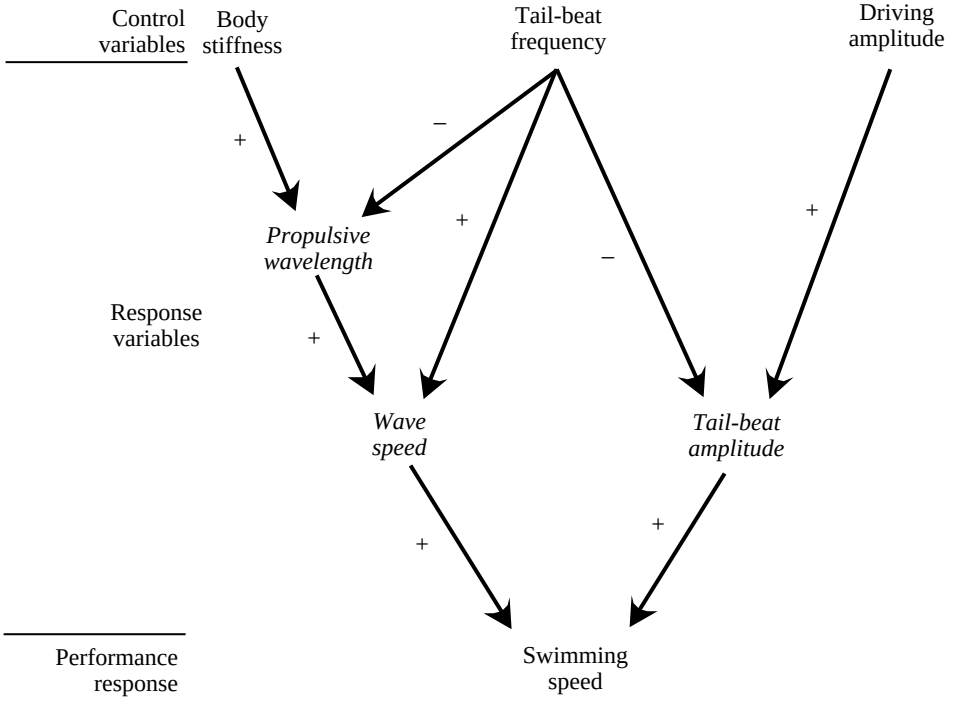

Fig. 11. The mechanical control of swimming speed: an integrated model. This flow chart serves the dual purpose of summarizing the relationships found for the model data and proposing a hypothetical model for how live fish control swimming speed. In order for live fish to operate within this framework, they must possess the ability to stiffen their bodies actively. Strong circumstantial evidence for this ability derives from the observation that live fish maintain a constant tail-beat amplitude and propulsive wavelength over a wide range of steady swimming speeds. Thus, as tail-beat frequency increases, either body stiffness or driving amplitude must increase to compensate, according to this model. A positive effect of one variable on another is indicated by a +. A negative effect is indicated by a −. Please note that tail-beat frequency has a positive relationship with wavespeed only when propulsive wavelength is actively held constant.

should be of great importance in determining the form of the propulsive wave. Stiffness of dead pumpkinseed sunfish bodies has been shown to affect undulatory wave motion (Long *et al.* 1994). In an attempt to build realistic models, we matched the Young's modulus in our second most flexible model (E=0.18 MPa) to that measured in the caudal region of a dead pumpkinseed sunfish (see Materials and methods for details). As a result, our stiffer models simulate a live fish using its muscles to stiffen the body *via* negative muscle work; it is important to note that the magnitude of negative work acting to stiffen the body has not been measured (see Van Leeuwen *et al.* 1990; Altringham *et al.* 1993; Rome *et al.* 1993).

By design, several kinematic variables of the axial wave are similar to those of live pumpkinseed sunfish. First, we chose driving frequencies (2–4 Hz) that were similar to the tail-beat frequencies measured in live pumpkinseed sunfish swimming at steady speeds. Second, we chose driving amplitudes that yielded rostral amplitudes similar to those of live pumpkinseed sunfish (reported as twice the rostral amplitude by Long *et al.* 1994). Thus, our three control variables (Young's modulus, driving frequency and rostral amplitude) match as closely as possible the same characteristics in live, swimming sunfish.

A striking difference between models and live sunfish is that in the models propulsive wavelength and tail-beat amplitude decrease with increasing driving frequency (Figs 4, 5). In live pumpkinseed sunfish, both propulsive wavelength and tail-beat amplitude are constant over a range of swimming speeds (Long *et al.* 1994). Rostral amplitude and tail-beat frequency are both positively correlated with swimming speed in live sunfish.

Thus, the most important functional distinction between live sunfish and the models is the control of undulatory wave speed; unlike live sunfish, the wave speed of each model cannot be altered. The fact that we had to use models of varying stiffnesses to establish a relationship between Young's modulus and wave speed (Fig. 7) supports the hypothesis that fish, which can change wave speed, are capable of changing the stiffness of their bodies. As discussed in the Introduction, a driven structure of fixed mass and stiffness must have a constant wave speed. This suggests that a live fish alters its body flexural stiffness and/or effective mass, which could change hydrodynamically. As suggested in past work (Altringham *et al.* 1993; Blight, 1976; Van Leeuwen *et al.* 1990), active lengthening of the caudal myomeres may enable a fish to modulate flexural stiffness. Because the models lack caudal force input, they cannot change wave speed. However, since the traveling undulatory wave powers swimming (see equation 2), the comparison of live sunfish and models swimming with identical wave speeds is an appropriate way to determine differences in propulsive performance (Fig. 10).

At a given wave speed, regional variation in Young's modulus may explain why live fish are more efficient swimmers than the models. The models, possessing a regionally constant Young's modulus, had a flexural stiffness ranging over three orders of magnitude. The disparity between precaudal and caudal flexural stiffness can be attributed to the tremendous difference in the second moment of area of these regions (Fig. 2). Although there may be hydrodynamic advantages to this design, it seems likely that a highly flexible caudal region would be susceptible to severe damping effects. In order to maintain a stiff caudal region, despite a small second moment of area, we predict that the caudal region of a fish possesses an elevated Young's modulus relative to that of the precaudal region.

It is also possible, although unlikely, that the significant difference in efficiencies of live fish and models may be caused by an artifact of hydrodynamic theory. When derived from elongated-body theory, the commonly used Froude efficiency, η (see equation 5, this paper), may be over-estimated in some circumstances (Cheng and Blickhan, 1994*b*). When compared with corrected values, Froude efficiences can differ by as much as 20 % at high ratios of swimming speed, u, to undulatory wave speed, c (Cheng and Blickhan, 1994*b*). This problem is unlikely, for two reasons, to be the source of the significantly higher Froude efficiency of live sunfish compared with that of models (Fig. 10). First, the mean Froude efficiency of live sunfish, which is more likely than the models to be over-estimated because of a greater ratio of u to c (0.73 *versus* 0.25, live and model sunfish, respectively), is over-estimated by less than 20 % in this case [approximately 10 % from Cheng and Blickhan's (1994*b*) Fig. 4]. Second, the difference in mean Froude efficiencies between live sunfish and models (35 %) is much larger than the difference caused by elongated-body theory (10 %).

Control of speed in live sunfish

On the basis of the mechanical behavior of our models, we can predict how live sunfish appear to violate simple mechanical theory (see Introduction). To maintain a constant tail-beat amplitude, we predict that live sunfish increase the driving amplitude of the undulatory wave in the precaudal region of the body, as seen in the models (Fig. 5B), and increase rostral amplitude with speed (Long *et al.* 1994). This is an alternative hypothesis for the lateral displacement of the rostrum, which may be a recoil response to the lateral motion of the body (Lighthill, 1970; Webb, 1988). To maintain a constant propulsive wavelength, we predict that live sunfish increase the stiffness of their bodies (Fig. 4C); increasing stiffness in models increases propulsive wavelength. In summary, we predict that, for live sunfish, the interaction of the three control variables increases swimming speed by modulating undulatory wave form (Fig. 11).

By extrapolation from the relationship between Young's modulus and the undulatory wave speed in the models (Fig. 7), we can predict what changes in the Young's modulus of a fish's body are necessary to increase wave speed and, thereby, to increase swimming speed. In the models, only changes in Young's modulus were sufficient to cause a change in the undulatory wave speed. This suggests that to elicit the observed increase in wave speed live sunfish must increase their apparent Young's modulus. We define the apparent Young's modulus as the combined active and passive resistance to bending relative to the body's second moment of

area, *I* (see also Wilson *et al.* 1991). When a fish is using none of its musculature to resist bending, the apparent Young's modulus is equal to the passive Young's modulus (that measured on a dead fish).

It is appropriate to extrapolate from the mechanical behavior of the models to that of live sunfish because the size, shape and kinematics of both are the same (although, as noted in the previous section, there are differences in performance and internal mechanics). First, it is necessary to correct for differences in body mass, as mass and stiffness are expected to affect undulatory wave speed in the following relationship (from Den Hartog, 1934), where we assume that resonance frequency is proportional to wave speed, *c*:

$$c \propto \sqrt{\frac{EI}{m}} , \qquad (7)$$

where *EI* is the flexural stiffness of the body and *m* is the body mass. Because the average wave speed of the model and live fish are statistically equivalent (Fig. 10A):

$$\sqrt{\frac{E_{\mathrm{a}}I}{m_{\mathrm{l}}}} = \sqrt{\frac{E_{\mathrm{m}}I}{m_{\mathrm{m}}}} , \qquad (8)$$

where E_a is the apparent Young's modulus of the live fish, E_{m} is the measured Young's modulus for the model, and m_{l} and m_{m} are the body masses of the live fish and the model, respectively. This yields the following relationship for the apparent modulus for the live fish:

$$E_{\mathrm{a}} = \frac{E_{\mathrm{m}}m_{\mathrm{l}}}{m_{\mathrm{m}}} , \qquad (9)$$

where $E_a = 1.316E_{\mathrm{m}}$ in our system. Correcting for differences in body mass, the equation for the relationship between Young's modulus and wave speed (c=166.736E_a +2.672) can be used to establish a value for the apparent Young's modulus of the caudal region of the body for a given wave speed. For live fish, we calculated a wave speed for each swimming speed from published kinematic data (Long *et al.* 1994). A value for apparent stiffness was calculated for each wave speed, so that a hypothetical relationship between swimming speed and apparent stiffness could be established (Fig. 12). According to this prediction, the apparent Young's modulus at high swimming speeds is 2–3 times the value for the passive Young's modulus.

In summary, this study demonstrates the mechanical feasibility of the following hypothesis: body stiffness controls speed and performance during steady, undulatory swimming. If live fish control body stiffness with negative muscle work, as proposed (Altringham *et al.* 1993; Blight, 1977; Long *et al.* 1994; Van Leeuwen *et al.* 1990), then they may alter undulatory wave form and swimming performance in a manner similar to that seen in our sunfish models. At the same time, this work underscores how little we know about the active and passive components of bending stiffness in fish bodies. Because of the difficulties of force measurement *in vivo*, our understanding of active muscle stiffness or stiffness changes with variable hydrodynamic loads awaits advances in experimental technique.

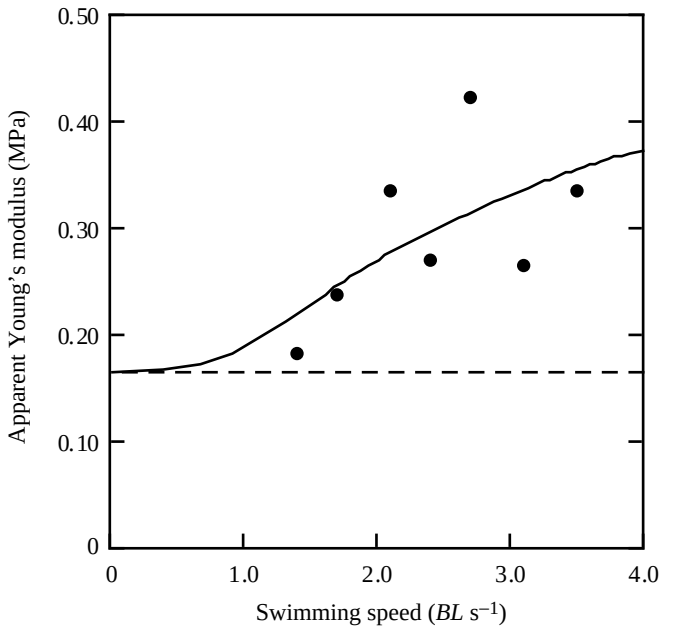

Fig. 12. Predicting increased body stiffness in live, swimming sunfish. Extrapolating from the results of the sunfish models, we predict that live pumpkinseed sunfish must double their apparent Young's modulus, relative to the passive (baseline) value, in order to swim at higher speeds. The points are calculated using the method described in the Discussion (equations 7–9); the dashed line represents the average passive Young's modulus measured in the caudal region of a dead pumpkinseed sunfish and is therefore the theoretical minimum (0.18 MPa). The solid line represents the predicted relationship between swimming speed and the apparent Young's modulus. *BL*, body length.

The authors would like to thank Steve Wainwright, founder of the BioDesign Studio, for his guidance and insight in the realm of mechanical modeling and fish locomotion. We also thank John Bertram, for his technical expertise and for the use of digitizing equipment during data analysis, Robert Suter, for his galvanometer design, Paul Webb, for his help in the refinement of our experiments and analysis, and Nick Boetticher, Sasha Cavanagh, Vynette Halthaufderhyde, Robert Suter, Steve Wainwright, Paul Webb and two anonymous reviewers for their comments on the manuscript. This work was supported by a grant to J.H.L. from the Office of Naval Research (N00014-93-1-0594). M.J.M. was supported by a research fellowship from the Undergraduate Research Summer Institute, Vassar College.

References

ALTRINGHAM, J. D., WARDLE, C. S. AND SMITH, C. I. (1993). Myotomal muscle function at different locations in the body of a swimming fish. *J. exp. Biol.* **182**, 191–206.

BAINBRIDGE, R. (1963). Caudal fin and body movement in the propulsion of some fish. *J. exp. Biol.* **40**, 23–56.

BLIGHT, A. R. (1976). Swimming with and without waves of contraction. *Nature* **264**, 352–354.

BLIGHT, A. R. (1977). The muscular control of vertebrate swimming movements. *Biol. Rev.* **52**, 181–218.

CHENG, J.-Y. AND BLICKHAN, R. (1994*a*). Bending moment distribution along swimming fish. *J. theor. Biol.* **168**, 337–348.

CHENG, J.-Y. AND BLICKHAN, R. (1994*b*). Note on the calculation of propeller efficiency using elongated body theory. *J. exp. Biol.* **192**, 169–177.

DEN HARTOG, J. P. (1934). *Mechanical Vibrations.* New York: McGraw-Hill Book Company, Inc.

DENNY, M. W. (1988). *Biology and the Mechanics of the Wave-Swept Environment.* Princeton, NJ: Princeton University Press.

HALLIDAY, D., RESNICK, R. AND WALKER, J. (1993). *Fundamentals of Physics.* New York: John Wiley and Sons, Inc.

HUNTER, J. R. AND ZWEIFEL, J. R. (1971). Swimming speed, tail-beat frequency, tail-beat amplitude and size in jack mackerel, *Trachyrus symmetricus*, and other fishes. *Fishery Bull. Fish Wildl. Serv. U.S.* **69**, 253–267.

JAYNE, B. C. AND LAUDER, G. V. (1994). Comparative morphology of the myomeres and axial skeleton in four genera of centrarchid fishes. *J. Morph.* **220**, 185–205.

JAYNE, B. C. AND LAUDER, G. V. (1995). Are muscle fibers within fish myotomes activated synchronously? Patterns of recruitment within deep myomeric musculature during swimming in largemouth bass. *J. exp. Biol.* **198**, 805–815.

LIGHTHILL, M. J. (1970). Aquatic animal propulsion of high hydromechanical efficiency. *J. Fluid Mech.* **44**, 265–301.

LIGHTHILL, M. J. (1975). *Mathematical Biofluiddynamics.* Res. Conf. Nat. Sci. Found., 1973, New York Soc. Ind. Appl. Math. SIAM.

LONG, J. H., JR (1992). Stiffness and damping forces in the intervertebral joints of blue marlin (*Makaira nigricans*). *J. exp. Biol.* **162**, 131–155.

LONG, J. H., JR, MCHENRY, M. J. AND BOETTICHER, N. (1994). Undulatory swimming: how traveling waves are produced and modulated in sunfish (*Lepomis gibbosus*). *J. exp. Biol.* **192**, 129–145.

ROME, L. C., SWANK, D. AND CORDA, D. (1993). How fish power swimming. *Science* **261**, 340–343.

SIMMS, E. L. AND BURDICK, D. S. (1988). Profile analysis of variance as a tool for analyzing correlated responses in experimental ecology. *Biometr. J.* **2**, 229–242.

VAN LEEUWEN, J. L., LANKHEET, M. J. M., AKSTER, H. A. AND OSSE, J. W. M. (1990). Function of red axial muscles of carp (*Cyprinus carpio*): recruitment and normalized power output during swimming in different modes. *J. Zool., Lond.* **220**, 123–145.

VIDELER, J. J. (1993). *Fish Swimming*. London: Chapman & Hall.

VOGEL, S. (1981). *Life in Moving Fluids.* Boston: Willard Grant Press.

WAINWRIGHT, S. A. (1983). To bend a fish. In *Fish Biomechanics* (ed. P. Webb and D. Weihs) pp. 68–91. New York: Praeger.

WAINWRIGHT, S. A., BIGGS, W. D., CURREY, J. D. AND GOSLINE, J. M. (1976). *Mechanical Design in Organisms*. New York: John Wiley and Sons.

WASSERSUG, R. J. AND HOFF, K. S. (1985). The kinematics of swimming in anuran larvae. *J. exp. Biol.* **119**, 1–30.

WEBB, P. W. (1986). Kinematics of lake sturgeon, *Acipenser fulvescens*, at cruising speeds. *Can. J. Zool.* **64**, 2137–2141.

WEBB, P. W. (1988). 'Steady' swimming kinematics of tiger musky, an esociform accelerator and rainbow trout, a generalist cruiser. *J. exp. Biol.* **138**, 51–69.

WEBB, P. W., KOSTECKI, P. T. AND STEVENS, E. D. (1984). The effect of size and swimming speed on locomotor kinematics of rainbow trout. *J. exp. Biol.* **109**, 77–95.

WESTNEAT, M. W., HOESE, W., PELL, C. A. AND WAINWRIGHT, S. A. (1993). The horizontal septum: mechanics of force transfer in locomotion of scrombrid fishes (Scombridae, Perciformes). *J. Morph.* **217**, 183–204.

WILLIAMS, T. L., GRILLNER, S., SMOLJANINOV, V. V., WALLEN, P., KASHIN, S. AND ROSSIGNAL, S. (1989). Locomotion in lamprey and trout: the relative timing of activation and movement. *J. exp. Biol.* **143**, 559–566.

WILSON, J. F., MAHAJAN, U., WAINWRIGHT, S. A. AND CRONER, L. J. (1991). A continuum model of elephant trunks. *J. Biomech. Eng.* **113**, 79–84.

WU, T. Y. (1977). Introduction to the scaling of aquatic animal locomotion. In *Scale Effects in Animal Locomotion* (ed. T. J. Pedley), pp. 203–232. New York: Academic Press.